RESEARCH ARTICLE

Unraveling bulk defects in high-quality c-Si material via TIDLS

Simone Bernardini[1], Tine U. Nærland[1], Adrienne L. Blum[2], Gianluca Coletti[3,4] and Mariana I. Bertoni[1] *

[1] Arizona State University, Tempe, AZ 85281, USA
[2] Sinton Instruments, Boulder, CO 80301, USA
[3] Energy Research Centre of the Netherlands, Petten 1755 LE, The Netherlands
[4] The University of New South Wales, Sydney, 2052NSW, Australia

ABSTRACT

The current trend in silicon photovoltaics moving towards high-quality thin mono-crystalline silicon substrates sets a new challenge for the understanding of recombination mechanisms limiting the final performance of solar cells. Temperature- and injection-dependent lifetime spectroscopy (TIDLS) has been shown to be a promising method for studying of high-quality material with lifetime above 10 ms where the concentration of electrically active defects is well below the sensitivity of the most well-known characterization techniques. In particular, when coupled with the Shockley–Read–Hall lifetime recombination model, TIDLS is capable of providing the most important defects' parameters including their energy level and concentration. In this contribution, we show that for a high-quality silicon material, a thorough evaluation of the surface recombination velocity (SRV) temperature- and injection dependence is crucial for an accurate identification of the defects contained in the bulk. A new methodology for the analysis of TIDLS data, called defect parameters contour mapping, is introduced for the first time. By applying it to high-quality n-type float zone c-Si samples passivated by a-Si:H(i) or an a-Si:H(i)/a-Si:H(n) stack, we are able to assert the presence of defects in high lifetime materials in a range of concentration unachievable by any other characterization technique thus far. Copyright © 2016 John Wiley & Sons, Ltd.

1. INTRODUCTION

In the last few years, research on silicon photovoltaic has strongly shifted toward high-quality mono-crystalline silicon material driven by the need of continuously pushing the efficiency/cost ratio.

As the quality of PV silicon increases, the problem of detecting small concentration of impurities below the sensitivity of the currently available experimental techniques has emerged. Lifetime spectroscopy (LS), which probes the recombination of injected minority charge carriers, has the clear advantage over other traditional methods of analyzing only those defect centers which contribute to the total recombination rate. Furthermore, as the measured lifetime depends not only on the defect concentration N_t but on its product with either the electron or the hole capture cross section—σ_n and σ_p, respectively—all LS

methods can achieve an extremely high sensitivity to electrically active defects [1].

Temperature- and injection-dependent lifetime spectroscopy (TIDLS) represents the most advanced among the LS techniques [2]. Its capabilities have been extensively exploited in the last decade to extract information about the harmful defects in silicon material. In particular defects' parameters such as the defect energy level in the band gap E_t, the capture cross-section ratio k (σ_n/σ_p) and the T-dependence of σ_p and σ_n have been confirmed or even assessed for the first time thanks to this technique [2]–[3]. However, in all these previous reports, the samples analyzed had been intentionally contaminated with a concentration of metal impurities well above what is to be expected in an industrially relevant Si ingot grown for PV applications. Thus, a clear methodology for the identification of impurities

in a high quality crystal with unknown impurities is still lacking.

The main obstacle for this TIDLS analysis is that the temperature and injection dependence of the surface passivation, usually expressed through the surface recombination velocity (SRV) parameter, is superposed to the characteristic shape of the bulk lifetime. As the quality of the substrate increases, the SRV impact on the measured lifetime gets stronger and the identification of bulk defects more difficult [1]. However, we show in this work that if a thorough characterization of the SRV temperature and injection dependence is carried out, TIDLS sensitivity can be extended to a range of impurity concentrations inaccessible to any other characterization technique.

2. EXPERIMENT

Crystalline silicon (c-Si) *n*-type float zone (FZ) wafers with a resistivity of $2.8\,\Omega\,cm$, crystal orientation (100) and initial thickness of $250\,\mu m$ were used in this work to fabricate symmetrically passivated samples. The substrates were subjected to an initial cleaning procedure which included the use of RCA-b and Piranha solutions. A series of samples with different thickness were obtained by subsequent dipping of about 2 min into an acid-based solution. This resulted in a removal of approximately $20\,\mu m$ of material after every dip and a final range of sample thicknesses of $250 - 150\,\mu m$. A final dip in diluted hydrofluoric acid solution was performed right before the deposition to ensure the removal of the silicon dioxide layer which readily forms on the surface. The substrates were then double-side coated with ~50 nm of a-Si:H(i) via plasma-enhanced chemical deposition (PECVD) at $200\,°C$. A post-deposition thermal treatment at $280\,°C$ for 30 min in air was carried out in a muffle furnace to ensure the thermal stability of the a-Si:H(i) layers during the samples measurements [4].

To study the electronic properties of the samples' interface as a function of T, the injection-dependent effective minority-lifetime (τ_{eff}) was measured using a Sinton Instruments WCT-120TS [5] which is equipped with a heating stage that allows the tool to work in a range of temperatures from 25 to $230\,°C$. Data were acquired by changing the temperature of the stage manually in steps of $10\,°C$ both as the temperature was increased and decreased to verify that no structural modification happens in the samples during the temperature cycle. The thermal stability of the samples was confirmed by the matching of τ_{eff} values at room T before and after carrying out a temperature cycle. Note that a small discrepancy was found along the two parts of the temperature cycle which we attributed to the temperature inhomogeneity on the stage being more pronounced in the first part of the temperature cycle, that is, when the temperature is increasing, because during the T-decreasing part the tool has usually more time to readjust. For this reason, in this work we only refer to data acquired during the decreasing part of the cycle with temperature going from 230 to $25\,°C$.

After the first cycle of lifetime acquisitions, the samples were subjected to a second cleaning cycle before a layer of *n*-doped a-Si:H(n) 10 nm thick was deposited via PECVD on both sides on top of the pre-existing a-Si:H(i) layer at $250\,°C$; no further annealing was carried out before the lifetime measures were repeated.

Given the high values of τ_{eff} obtained from the samples with both passivation schemes, all data were acquired in transient mode. Every measure was averaged over 20 acquisitions to improve the signal to noise ratio.

3. RESULTS AND DISCUSSION

In the following section, we discuss the results obtained from *T*-dependent photoconductance decay measurements on samples with different passivation schemes. The reported SRV values are experimentally obtained by measuring samples with different thickness so that no assumptions are made a priori on the quality of the substrate or the passivation level.

For double-side coated samples with a minority carrier diffusion length greater than the sample width (W), and for sufficient low SRV, we can express the effective lifetime as [6]

$$\frac{1}{\tau_{eff}(\Delta n, T)} = \frac{1}{\tau_{bulk}(\Delta n, T)} + \frac{2 \cdot SRV(\Delta n, T)}{W} \quad (1)$$

where τ_{eff} is the effective lifetime and τ_{bulk} is the bulk lifetime which can also be expressed according to the following equation

$$\frac{1}{\tau_{bulk}} = \frac{1}{\tau_{SRH}} + \frac{1}{\tau_{Auger}} + \frac{1}{\tau_{rad}} = \frac{1}{\tau_{SRH}} + \frac{1}{\tau_{int}} \quad (2)$$

where τ_{SRH} is the Shockley–Read–Hall lifetime, τ_{Auger} is the Auger lifetime, τ_{rad} is the radiative lifetime and τ_{int} is the intrinsic lifetime which is given by the inverse sum of the last two terms.

Equation (1) allows separating the contribution given to τ_{eff} by the recombination mechanisms happening in the bulk of the material from those happening at the interface thanks to the variation of the substrate's thickness. However, in order to measure the bulk lifetime, SRV values have to be evaluated at every temperature and injection level. The study of the nature of the recombination mechanism happening at the interface and its dependence on temperature will be treated separately in a different paper.

Equation (2) reveals the different recombination mechanisms that happen within the bulk of the material distinguishing among "intrinsic" processes, that is, Auger and radiative recombination mechanisms, which cannot be mitigated, and "extrinsic" processes, that is, defect-assisted SRH recombination. In this work, we will make use of the advanced parameterization proposed by Richter *et al.* [7] for the intrinsic recombination in crystalline

silicon. Note that the *T*-dependence of the parameters used to model these processes have been experimentally determined for a window of injections and temperatures narrower than the one considered here. In particular, the radiative recombination coefficient $B(T)$ has only recently been evaluated to a temperature up to 90 °C [8]. The results were found to agree well with the previously established data published by Trupke *et al.* [9], on which our analysis is based, as $B(T)$ values at higher temperatures were extrapolated from a parameterization of data reported in that work. Similarly, Auger recombination *T*-dependence has not been extensively studied. Recently Wang *et al.* evaluated the ambipolar Auger coefficient C_a across a temperature range from −30 to 200 °C [10] but only at a very high injection level of 5×10^{16} cm^{-3}. Based on this, we expect some discrepancy and thus higher errors at temperatures above 100 °C. The Auger recombination *T*-dependence in a broader range of injection level will be the subject of our investigation in a different paper.

Contrary to the intrinsic recombination processes, SRH lifetime modeling is very well-established based on the Shockley–Read–Hall theory [11]-[12] of carrier generation and recombination at a single defect level with energy E_t according to the equation

$$\tau_{SRH} = \frac{\tau_{n0}(p_0 + p_1 + \Delta n) + \tau_{p0}(n_0 + n_1 + \Delta n)}{p_0 + n_0 + \Delta n} \quad (3)$$

where τ_{n0} and τ_{p0} are the capture time constants and n_0 and p_0 the equilibrium densities of electrons and holes, respectively. As trapping is assumed to be negligible, the excess carrier densities of electrons and holes are equal ($\Delta n = \Delta p$). Finally, the so-called SRH densities n_1 and p_1 are given by

$$n_1 = N_C exp\left(-\frac{E_C - E_t}{kT}\right), \ p_1 = N_V exp\left(-\frac{E_t - E_V}{kT}\right) \quad (4)$$

where E_t is the energy level of the recombination center, E_C and E_V are the energies of the conduction and the valence band edge, respectively, and N_C and N_V are the effective densities of states in the conduction and the valence band [13], respectively. The time constants τ_{n0} and τ_{p0} for the capture of electrons and holes in the defect state are proportional to the inverse product of the defect concentration N_t and the capture cross sections σ_n and σ_p for electrons and holes:

$$\tau_{p0} = \left(N_t \sigma_p v_{th}\right)^{-1}, \ \tau_{n0} = \left(N_t \sigma_n v_{th}\right)^{-1} \quad (5)$$

where v_{th} is the thermal velocity for either electrons or holes [13]. Another important defect parameter is the capture cross section ratio k defined by the equation

$$k \equiv \frac{\sigma_n}{\sigma_p} = \frac{\tau_{p0}}{\tau_{n0}} \quad (6)$$

(A) Passivation by a-Si:H(i)

The τ_{eff} versus injection level curves at different temperatures for the thickest sample ($W = 250\,\mu$m) passivated with a-Si:H(i) are shown in Figure 1. Samples with smaller thickness show a slightly lower effective lifetime consistently with Eq. (1) but an overall similar behavior.

We notice that the *T*-dependence of τ_{eff} varies with the carrier injection level. For this reason, we extract *T*-traces for each injection level indicated by a dashed vertical line. The results are shown in Figure 2. After an initial increment with temperatures up to 60 °C, the effective lifetime is found to decrease monotonically with increasing *T*. This trend tends to disappear with increasing injection level as the effective lifetime starts to be mostly limited by the temperature-independent Auger recombination mechanism.

Similar τ_{eff} trends have been recently reported by J. P. Seif *et al.* [14] and have been linked to the *T*-dependence
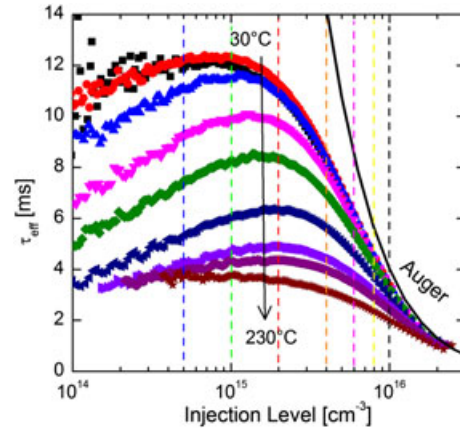

Figure 1. Effective minority-carrier lifetime as function of injection level at temperatures with 20 °C step size for a high-quality Si sample 250-μm-thick passivated with 50 nm of a-Si:H(i).
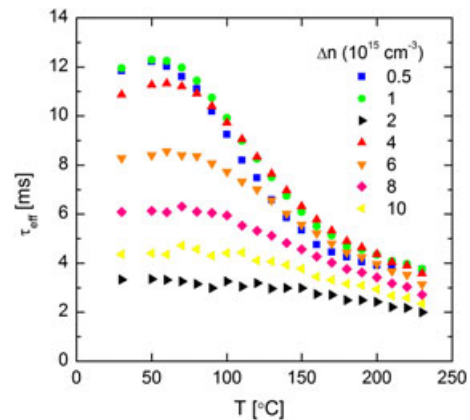

Figure 2. Temperature dependence of τ_{eff} at different injection levels for a high-quality Si sample 250-μm-thick passivated with 50 nm of a-Si:H(i).

of recombination mechanisms happening at the c-Si surface rather than in the c-Si bulk. Thanks to the experimental evaluation of SRV carried out according to Eq. (1), we are now able to prove that this assumption is correct. Figure 3 shows that at room temperature an outstanding SRV below 0.5 cm/s at an injection level equal to 10^{15} cm^{-3} is obtained—to the authors' knowledge this represents the best passivation provided by amorphous silicon on *n*-type substrates reported up to date, in line with results by S. Herasimenka *et al.* [15] who reported a record V_{OC} for a device with a similar passivation scheme. SRV is then found to increase as the temperature rises above 100 °C although never moving above the value of 5 cm/s in the temperature and injection level ranges evaluated here.

The SRV *T*-dependence corresponds well to the diminishing τ_{eff} from Figure 2, and the surface recombination is therefore expected to dominate at high temperature. To confirm this finding, we take the SRV term out of the effective lifetime according to Eq. (1) and plot the bulk lifetime versus injection level. The results are shown in Figure 4 along with τ_{eff} at 30 °C for a direct comparison.

The comparison of τ_{eff} and τ_{bulk} at 30 °C shows that the latter exhibit a stronger injection dependence. Furthermore and more importantly, the *T*-dependence is now completely reversed compared to the effective lifetime and τ_{bulk} is found to increase with temperature as it would be expected from the exponential temperature dependence of the SRH density p_1 in Eq. (4). Interestingly, bulk lifetime is found to perfectly match the Auger limit at 150 °C while any curve at higher temperature (not shown here) is seen to sit beyond that limit. This is probably due to the uncertainty of the Auger recombination coefficient at high temperatures as mentioned at the beginning of this discussion.

We will show in section IV that the discrepancy between τ_{eff} and τ_{bulk} is of the utmost importance for the identification of deleterious defects in the bulk of high-quality material. However, because of the model limitations we
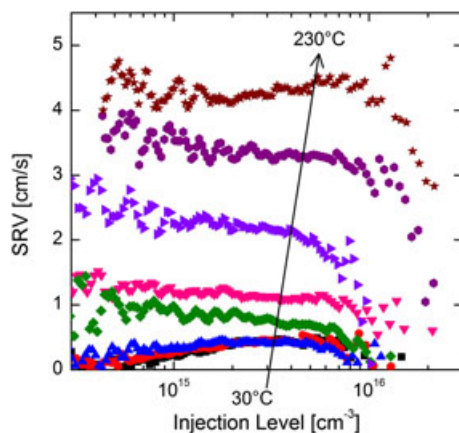

Figure 4. Bulk lifetime as function of injection level at temperatures with 20 °C step size up to 150 °C for samples passivated with a-Si:H(i). τ_{eff} at room temperature (empty squares) is reproduced for comparison.

will restrain our analysis to a range of temperatures from 30 to 150 °C.

(B) Passivation by a-Si:H(i)/a-Si:H(n) stack layer

As in real devices such as silicon heterojunction solar cells (SHJ), the intrinsic a-Si:H layer is always coupled to a doped a-Si:H layer working as a carrier-selective contact, we proceeded with the deposition of a 10-nm-thick layer of a-Si:H(n) with an estimated doping of 10^{19} cm^{-3} on top of the same samples used for the first part of this work.

The τ_{eff} versus injection level curves at different temperatures for the thickest sample passivated with a-Si:H(i)/a-Si:H(n) stack are shown in Figure 5. As in the previous case, samples with lower thickness show a similar trend at slightly lower values accordingly to Eq. (1).

Similarly to samples coated only with a-Si:H(i), we notice that the *T*-dependence of τ_{eff} varies with the carrier

Figure 3. Surface recombination velocity as function of injection level at different temperatures with 20 °C step size for high-quality Si samples coated with 50 nm of a-Si:H(i).
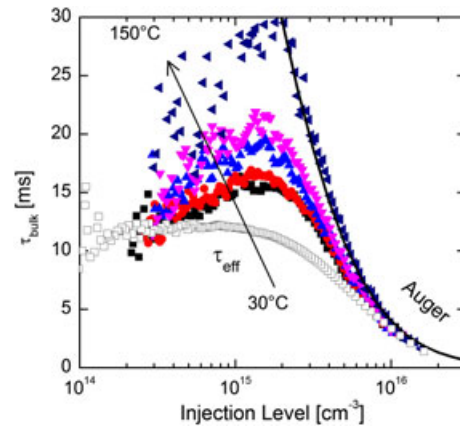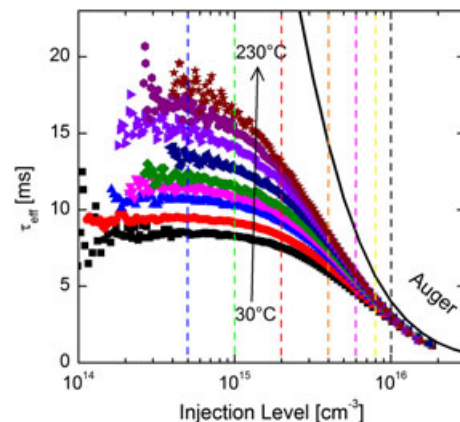

Figure 5. Effective minority-carrier lifetime as function of injection level at different temperatures with 20 °C step size for a high-quality Si sample passivated with a-Si:H(i)/a-Si:H(n).

injection level and so we extract *T*-traces for each injection level indicated by a dashed line. Results are shown in Figure 6.

These results are in line with what has been recently reported for similar samples at *T* below [16] and above [14] [17] room temperature. It is worth noting that in the case of samples coated with the a-Si:H(i)/a-Si:H(n) stack the effective lifetime already show the increasing *T*-dependence seen for τ_{bulk} in Figure 4 so that a different SRV behavior with temperature can already be expected.

As shown in Figure 7, the SRV results on samples coated with the stack a-Si:H(i)/a-Si:H(n) are consistently below 1.5 cm/s in the whole range of temperatures.

The resulting bulk lifetime is shown in Figure 8. Although we would expect SRV to have a lower impact on τ_{eff} compared to samples coated with a-Si:H(i), bulk lifetime is still significantly different from the τ_{eff} shown in Figure 5 as can be seen from a comparison with the effective lifetime at 30 °C presented in Figure 8.
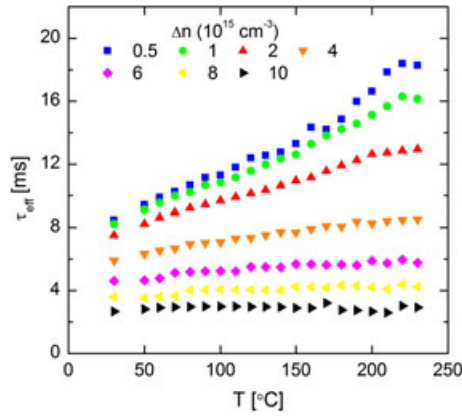

Figure 6. Temperature dependence of τ_{eff} at different injection levels for a high-quality Si sample passivated with a-Si:H(i)/a-Si:H(n).
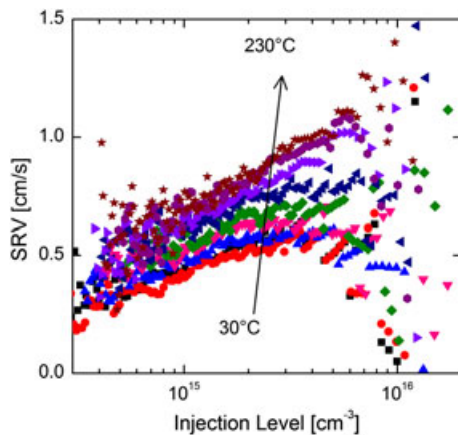

Figure 7. Surface recombination velocity as function of injection level at different temperatures with 20 °C step size for high-quality Si samples coated with a-Si:H(i)/a-Si:H(n).
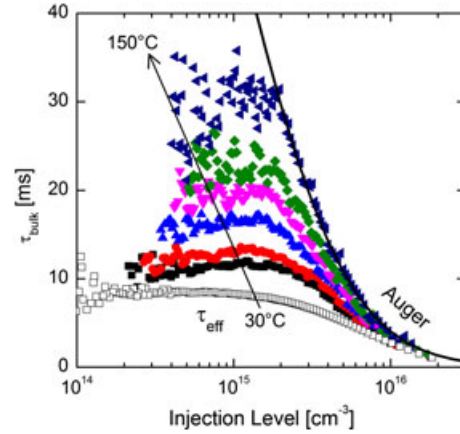

Figure 8. Bulk lifetime as function of injection level at different temperatures with 20 °C step size up to 150 °C for samples passivated with a-Si:H(i)/a-Si:H(n). τ_{eff} at room temperature (empty squares) is reproduced for comparison.

Remarkably, the results are very similar to those shown in Figure 4 which corroborates the validity of this method for τ_{bulk} extrapolation. Again, the bulk lifetime is found to match the Auger limit at 150 °C while any curve at higher temperature sits beyond that limit and is not shown for the sake of clarity.

4. MODELING OF DATA

In the following section we will introduce a method we denominate defect parameters contour mapping (DPCM) which can be used to complement a TIDLS analysis to quickly determine the most likely lifetime limiting defect in PV silicon samples. This method builds upon the framework presented by S. Rein [18] and is extended to represent in a single comprehensive plot the quality of the TIDLS data fitting obtained in the whole parameter space. DPCM further allows for an immediate evaluation and screening of all the defect levels reported in literature, which becomes very useful especially when the source of contamination is unknown.

When applied to our experimental data, this analysis proves that the generally accepted assumption $\tau_{eff} \approx \tau_{bulk}$ does not hold for high-quality material and that a direct measurement of SRV as function of temperature and injection is required.

The method is built upon the use of contour plots to evaluate the quality of the fitting obtained using the SRH theory (Eqs. (3), (4), (5) and (6)) applied to the measured lifetime curves for a wide range of E_t and *k* values so to account for possible combinations of parameters not yet associated with defects reported in literature. In order to do so, our main assumption is that the lifetime is dominated by only one defect level in the whole range of temperature evaluated. The lifetime versus injection level curve is initially simulated at room temperature for every (*k*, E_t) combination varying the time constants τ_{p0} and τ_{n0} until a best

fit of the experimental data is obtained. The quality of the fit, represented by lighter color in the contour plot, is determined by calculating an *Average Residual Value* (%) over five different injection levels over five different temperatures according to the equation

$$\text{Average Residual Value } (\%)$$
$$= \left(\sum_{i=1}^{n} \left(\sum_{j=1}^{m} \frac{|\tau_{measured,j} - \tau_{model,j}|}{\tau_{measured,j}} \right) / m \right) / n \quad (7)$$

where n is the number of lifetime curves at different temperatures, m is the number of injection level values at which the fit is evaluated, $\tau_{measured}$ can be either the effective lifetime or the bulk lifetime, and τ_{model} is obtained accordingly to the procedure explained in Section III. Normally, when fitting lifetime with the SRH model, $\Sigma(\tau_{measured} - \tau_{model})^2$ is minimized. However, when the lifetime crosses several orders of magnitudes, this method unintentionally allocates larger weight to the higher-value lifetime data. To avoid this problem, $\Sigma[|\tau_{measured} - \tau_{model}|/\tau_{measured}]$ was minimized in the fitting to determine the optimal τ_{p0} and τ_{n0} in this work. Furthermore, taking the absolute value of $\tau_{measured} - \tau_{model}$ instead of the square value enables the assessment of a true modeled-to-measured residual percentage.

The choice of the number of injection levels to be compared and their values can be modified to account for characteristic features in the lifetime curve at a certain injection level which would help obtaining a more univocal fit. However, as our lifetime curves do not show any particularly relevant feature along the whole injection range, we simply choose five values evenly spaced across $5 \times 10^{14} - 1 \times 10^{16}$ cm^{-3}. Once the time constants associated with the best fit (τ_{p0} and τ_{n0}) at room temperature have been assessed, they are kept fixed and subsequently employed

to evaluate the fit over four more different temperatures over the range 30 – 150 °C. The *Average Residual Value* is calculated for each of the lifetime curve associated with a certain temperature and then averaged as shown in Eq. (7). We acknowledge that keeping the time constants fixed for different temperatures is equal to assuming σ_p and σ_n— and thus k—to be T-independent while for many metal impurities this is not the case. However, we account for this temperature dependence by associating an error to the k value reported for every known defect level. In this way, we can still present all the results of the TIDLS data fitting in a single plot, which is the main goal of the DPCM method. Note that in order to accurately estimate the error associated with the temperature dependence of k, both σ_p and σ_n T-dependence needs to be known—something that is available for very few defects. Based on the T-dependence of $\sigma_{n,p}$ associated with various capture mechanisms reported by S. Rein [18] and K. Graff [19], and given the limited T range taken into account, we can estimate this error to be at maximum 60% for the case of Iron. This number will vary substantially with the metal of interest.

In Figures 9 and 10, the metal defects with well-established parameters' values taken from [4,5,25–32] are depicted on the graph enabling us to readily verify which ones among these defects are the most likely to represent the source of recombination within the bulk of the material. The list of defects shown in the contour plot could be easily updated should new defects' parameters be established.

In Figure 9, we show the contour plot obtained following the procedure described above for the τ_{eff} data of samples coated with a-Si:H(i) shown in Figure 1. It appears immediately that there are no E_t and k combinations for which a good fit quality is obtained as the *Average Residual Value* is always above the value of 18%.

The situation changes substantially when we repeat the procedure using the τ_{bulk} data shown in Figures 4 and 8
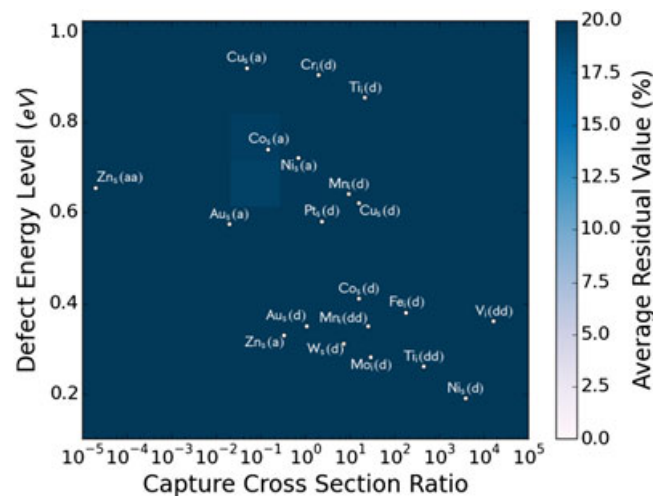

Figure 9. Contour plot showing the quality of fit for τ_{eff} of a-Si:H(i) coated samples averaged over different temperatures across a range from 30 to 150 °C. The DPCM analysis using the effective lifetime draws no good fit to the experimental TIDLS data.
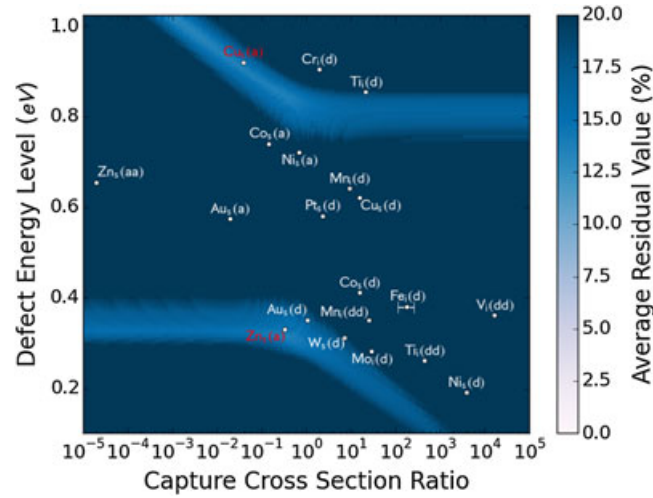
Figure 10. Contour plot showing the quality of fit for τ_{bulk} averaged over different temperatures across a range from 30 to 150 °C. Defects for which the best is obtained are shown in red. An error of 60% is shown for Fe$_i$(d) as a representative for the uncertainty associated with the k values of defect level because of its temperature dependence. The DPCM analysis using the bulk lifetime reveals areas of good fit for multiple combinations of E$_t$ and k (white contours).

rather than τ_{eff}. Some characteristic bright areas appear in the contour plot shown in Figure 10 corresponding to an *Average Residual Value below 11%* which can be considered as an acceptable fit taking into the errors associated with the method of measurements [33] and uncertainties in models employed [14]. A 60% error is shown for the k value of Fe$_i$(d) as a representative for the uncertainty of defect levels because of its temperature dependence [26]. It is easy to verify that even accounting for such a high level of uncertainty our method is still accurate enough to discriminate among different defect levels.

As expected, the (k, E_t) solutions resulting in a good fit are symmetric for k-values close to unity because defects with the same energy level distance from either the valence or the conduction band have virtually the same recombination strength [2]. The bright area in the upper half of the bandgap becomes E_t-independent when $k > 1$, i.e., $\sigma_n > \sigma_p$, since all the electrons accessible by the defect level are already made available and any further increment of σ_n does not correspond to an increment in the recombination strength. The same explanation holds for the E_t-independent bright region in the lower half of the bandgap for holes when $k < 1$, i.e., $\sigma_p > \sigma_n$.

Given the narrowness of the bright areas, we can shrink the list of possible harmful defects among those reported on the graph to just one defect in the lower half of the bandgap and one in the upper half, respectively, the single acceptor state of Zn$_s$ and the single acceptor state of Cu$_s$ (shown in red in Figure 10). Thanks to the knowledge of τ_{p0} from the modeling and using the hole capture cross sections σ_p reported in [4] and [29] for these defects we can calculate the defect density N_t from Eq. (5) with the thermal velocity $v_{th} = 2.1 \times 10^7$ cm/s. For the Zn$_s$ defect, we obtained an N_t of 1.4×10^9 cm^{-3}. For the Cu$_s$ defect, we obtained an N_t of 1.6×10^{10} cm^{-3}. In an attempt to verify the E_t level of the defect of interest, we analyzed the

samples with deep-level transient spectroscopy (DLTS) which is accepted to be one of the most sensitive methods for characterization of electrically active defects: As DLTS is sensitive to a concentration of defects above 10^{12} cm^{-3} for samples with a doping of ~10^{15} cm^{-3}, no impurities were detected in our specimens further corroborating the extraordinary sensitivity of the TIDLS method. While copper's harmful effect has been previously assessed [26,29] and its presence in silicon would not be surprising, zinc has been thought to be an innocuous impurity in device fabrication as its low evaporation temperature—lower than its melting temperature—makes it evaporate during heat treatments of the wafers so that it has never been found in the bulk of processed samples but only on polished surfaces of as-received material [26]. Our results show that, contrarily to what previously believed, a small concentration of zinc could actually be present in the bulk of high-quality c-Si and contribute to the recombination mechanisms.

It must be noticed that, although at room temperature a very good fit of the experimental bulk lifetime is obtained by modeling with only one defect's parameters, things could be different at higher temperatures where other defects can get activated because of the shift of Fermi energy in the Si bandgap which would in turn lead to a general worsening of the fit.

5. CONCLUSIONS

The effective lifetime temperature and injection dependence of high quality *n*-type FZ c-Si samples for several passivation schemes was experimentally evaluated. The τ_{eff} *T*-dependence was found to be strongly influenced by the properties at the interface even when a very good level of passivation is provided.

A record low SRV of 0.5 cm/s is achieved with a double-side 50 nm a-Si:H(i) layer at room temperature at the injection level of 10^{15} cm^{-3} which is then found to increase at T above 100 °C. Addition of 10 nm a-Si:H(n) layer on both surfaces helps preventing this increment and maintains SRV below 1 cm/s in the range of temperature over 30 – 230 °C.

We demonstrate that, even in case of ideal surface passivation, the full SRV temperature and injection characterization is necessary for the correct evaluation of bulk lifetime and that the simple assumption $\tau_{eff} \approx \tau_{bulk}$ is hence not valid for high-quality material. Furthermore, we establish a new methodology denominated defect parameter contour mapping (DPCM) to evaluate possible harmful defects contained in the material by mean of contour plots showing the quality of fit among experimental and simulated TIDLS data. By applying this method to τ_{bulk} data, we were able to identify two possible impurities as responsible for the recombination in the bulk and assess their concentrations. This work exhibits the path to extend the TIDLS capabilities to an extraordinary level of sensitivity and asserts it as the only experimental technique available hitherto for the characterization of defects in high-quality Si material.

ACKNOWLEDGEMENTS

REFERENCES

1. Rein S, Rehrl T, Warta W, Glunz SW. Lifetime spectroscopy for defect characterization: systematic analysis of the possibilities and restrictions. *Journal of Applied Physics* 2002; **91**: 2059–2070. DOI:10.1063/1.1428095

2. Schmidt J. Temperature- and injection-dependent lifetime spectroscopy for the characterization of defect centers in semiconductors. *Applied Physics Letters* 2003; **82**: 2178–2180. DOI:10.1063/1.1563830

3. Macdonald D, Tan J, Trupke T. Imaging interstitial iron concentrations in boron-doped crystalline silicon using photoluminescence. *Journal of Applied Physics* 2008; **103**(7): 073710. DOI:10.1063/1.2903895

4. Macdonald DH, Geerligs LJ. Recombination activity of interstitial iron and other transition metal point defects in p- and n-type crystalline silicon. *Applied Physics Letters* 2004; **85**: 4061–4063. DOI:10.1063/1.1812833

5. Diez S, Rein S, Roth T, Glunz SW. Cobalt related defect levels in silicon analyzed by temperature- and injection-dependent lifetime spectroscopy. *Journal of Applied Physics* 2007; **101**(033710): 1–6. DOI:10.1063/1.2433743

6. Dubois S, Palais O, Ribeyron PJ. Determination at 300 K of the hole capture cross section of chromium–boron pairs in p-type silicon. *Applied Physics Letters* 2006; **89**: 232112–232115. DOI:10.1063/1.2402261

7. Schmidt J, Krain R, Bothe K, Pensl G, Beljakowa S. Recombination activity of interstitial chromium and chromium–boron pairs in silicon. *Journal of Applied Physics* 2007; **102**: 123701. DOI:10.1063/1.2822452

8. Hystad M, Modanese C, Di Sabatino M, Arnberg L. Distribution and impact of chromium in compensated solar grade silicon. *Solar Energy Materials and Solar Cells* 2012; **103**: 140–146. DOI:10.1016/j.solmat.2012.04.033

9. Paudyal BB, McIntosh KR, Macdonald DH. Temperature dependent carrier lifetime studies on Ti-doped multicrystalline silicon. *Journal of Applied Physics* 2009; **105**: 124510. DOI:10.1063/1.3139286

10. Paudyal BB, McIntosh KR, Macdonald DH, Coletti G. Temperature dependent carrier lifetime studies of Mo in crystalline silicon. *Journal of Applied Physics* 2010; **107**: 054511. DOI:10.1063/1.3309833

11. De Wolf S, Kondo M. Nature of doped a-Si:H/c-Si interface recombination. *Journal of Applied Physics* 2009; **105**: 103707. DOI:10.1063/1.3129578

12. Sinton RA, Cuevas A. Contactless determination of current–voltage characteristics and minority carrier lifetimes in semiconductors from quasi-steady-state photoconductance data. *Applied Physics Letters* 1996; **69**: 2510–2513. DOI:10.1063/1.117723

13. Sproul AB. Dimensionless solution of the equation describing the effect of surface recombination on carrier decay in semiconductors. *Journal of Applied Physics* 1994; **76**: 2851–2855. DOI:10.1063/1.357521

14. Richter A, Glunz S, Werner F, Schmidt J, Cuevas A. Improved quantitative description of Auger recombination in crystalline silicon. *Physical Review B* 2012; **86**: 165202. DOI:10.1103/PhysRevB.86.165202

15. Nguyen HT, Baker-Finch SC, Macdonald DH. Temperature dependence of the radiative recombination coefficient in crystalline silicon from spectral photoluminescence. *Applied Physics Letters* 2014; **104**: 112105. DOI:10.1063/1.4869295

16. Trupke T, Green MA, Würfel P, Altermatt PP, Wang A, Zhao J, Corkish R. Temperature dependence of the radiative recombination coefficient of intrinsic crystalline silicon. *Journal of Applied Physics* 2003; **94**: 4930. DOI:10.1063/1.1610231

17. Wang S, Macdonald DH. Temperature dependence of Auger recombination in highly injected crystalline silicon. *Journal of Applied Physics* 2012; **112**: 113708. DOI:10.1063/1.4768900

18. Shockley W, Read WT. Statistics of the recombinations of holes and electrons. *Physical Review* 1952; **87**: 835–842. DOI:10.1103/PhysRev.87.835

19. Hall RN. Electron–hole recombination in germanium. *Physical Review* 1952; **87**: 387. DOI:10.1103/PhysRev.87.387

20. Green MA. Intrinsic concentration, effective densities of states, and effective mass in silicon. *Journal of Applied Physics* 1990; **67**: 2944–2955. DOI:10.1063/1.345414

21. Seif JP, Krishnamani G, Demaurex B, Ballif C, De Wolf S. Amorphous/crystalline silicon interface passivation: ambient-temperature dependence and implications for solar cell performance. *IEEE Journal of Photovoltaics* 2015; **5**: 718–724. DOI:10.1109/JPHOTOV.2015.2397602

22. Herasimenka SY, Tracy CJ, Sharma V, Vulic N, Dauksher WJ, Bowden SG. Surface passivation of n-type c-Si wafers by a-Si/SiO2/SiNx stack with <1 cm/s effective surface recombination velocity. *Applied Physics Letters* 2013; **103**: 183903. DOI:10.1063/1.4827821

23. Courtois G, Bruneau B, Sobkowicz IP, Salomon A, Cabarrocas PRI. Carrier lifetime measurements by photoconductance at low temperature on passivated crystalline silicon wafers. *MRS Online Proceedings Library* 2013; **1536**: 119–125.

24. Sinton RA, Blum AL, Swirhun JS. Overview and latest developments in photoconductance lifetime measurements in silicon. *Solid State Phenomena* 2014; **205-206**: 103–109. DOI:10.4028/www.scientific.net/SSP.205-206.103

25. Rein S. *Lifetime Spectroscopy: A Method of Defect Characterization in Silicon for Photovoltaic Applications*. Springer: Berlin, 2005.

26. Graff K. *Metal Impurities in Silicon-Device Fabrication*. Springer: Berlin, 1999.

27. Wang AC, Sah CT. Complete electrical characterization of recombination properties of titanium in silicon. *Journal of Applied Physics* 1984; **56**: 1021–1031. DOI:10.1063/1.334095

28. Fazzio A, Caldas MJ, Zunger A. Electronic structure of copper, silver, and gold impurities in silicon. *Physical Review B* 1985; **32**: 934–954. DOI: 10.1103/PhysRevB.32.934

29. Macdonald D, Brendle W, Cuevas A, Istratov AA. *"Injection dependent lifetime studies of copper precipitates in silicon,"* *Proceedings of 12th Workshop Crystalline Silicon Solar Cell Materials and Processes*. Golden: Colorado, 2002.

30. Roth T, Rosenits P, Diez S, Glunz SW, Macdonald D, Beljakowa S, Pensl G. Electronic properties and dopant pairing behavior of manganese in boron-doped silicon. *Journal of Applied Physics* 2007; **102**: 103716. DOI:10.1063/1.2812698

31. Kwon YK, Ishikawa T, Kuwano H. Properties of platinum-associated deep levels in silicon. *Journal of Applied Physics* 1987; **61**: 1055–1058. DOI:10.1063/1.338197

32. Mishra K. Identification of Cr in p-type silicon using the minority carrier lifetime measurement by the surface photovoltage method. *Applied Physics Letters* 1996; **68**: 3281–3283. DOI:10.1063/1.116574

33. Blum AL, Swirhun JS, Sinton RA, Yan F, Herasimenka S, Roth T, Lauer K, Haunschild J, Lim B, Bothe K, Hameiri Z, Seipel B, Xiong R, Dhamrin M, Murphy JD. Interlaboratory study of eddy-current measurement of excess-carrier recombination lifetime. *IEEE Journal of Photovoltaics* 2014; **4**: 525–531. DOI: 10.1109/JPHOTOV.2013.2284375